nature materials

Article

https://doi.org/10.1038/s41563-023-01577-2

Metamaterial adhesives for programmable adhesion through reverse crack propagation

Received: 1 December 2021

Accepted: 4 May 2023

Published online: 22 June 2023

Check for updates

Dohgyu Hwang[1,2], Chanhong Lee[1], Xingwei Yang[3], Jose M. Pérez-González[4], Jason Finnegan[5], Bernard Lee[5], Eric J. Markvicka[5], Rong Long[3] & Michael D. Bartlett[1,2]

Adhesives are typically either strong and permanent or reversible with limited strength. However, current strategies to create strong yet reversible adhesives needed for wearable devices, robotics and material disassembly lack independent control of strength and release, require complex fabrication or only work in specific conditions. Here we report metamaterial adhesives that simultaneously achieve strong and releasable adhesion with spatially selectable adhesion strength through programmed cut architectures. Nonlinear cuts uniquely suppress crack propagation by forcing cracks to propagate backwards for 60× enhancement in adhesion, while allowing crack growth in the opposite direction for easy release and reusability. This mechanism functions in numerous adhesives on diverse substrates in wet and dry conditions and enables highly tunable adhesion with independently programmable adhesion strength in two directions simultaneously at any location. We create these multifunctional materials in a maskless, digital fabrication framework to rapidly customize adhesive characteristics with deterministic control for next-generation adhesives.

Adhesive strength is dictated by how cracks move across a bonded interface[1–4]. By suppressing crack propagation, strong adhesives are created but are difficult to remove, while reusable adhesives promote separation which limits strength. This makes adhesives commonly either permanent and strong or reversible with limited strength. However, many applications are increasingly in need of adhesives that overcome this trade-off in properties and require strong adhesion with easy removal and extended reuse. This seemingly paradoxical combination of properties is important in applications such as robotics for locomotion and grasping, wearable electronics for strong attachment yet easy removal of devices to monitor health and deliver drugs, and manufacturing for assembly and then disassembly to reduce waste, repurpose materials and aid in recycling[5–10].

Material approaches to control adhesion typically focus on tuning interfacial chemistry or dissipating mechanical energy[11–14]. These material-based mechanisms can result in very strong adhesives, but often do not have mechanisms for release, reusability or directionality (that is, high strength in one direction relative to another) because dissipation near the crack tip is similar in all directions. Geometry and stiffness also control adhesion. This is achieved through nano-to-micron-scale bioinspired surface features[15–21], passively varying stiffness through material patterning or actively varying stiffness with switchable adhesives[22–29], or adding incisions, cuts or discontinuities into adhesives[30–34]. These features blunt or trap cracks, which then reinitiate and propagate again in the original, forward direction[31]. This increases adhesion force but does not necessarily facilitate directionality or release. Directional strength can be achieved[35], but it is difficult to raise adhesion strength and directionality because geometric mechanisms typically result in adhesion strengths below material-based mechanisms. Strategies that leverage both material and geometric mechanisms through accessible fabrication approaches can open synergistic opportunities to systematically suppress crack

[1]Department of Mechanical Engineering, Soft Materials and Structures Lab, Virginia Tech, Blacksburg, VA, USA. [2]Macromolecules Innovation Institute, Virginia Tech, Blacksburg, VA, USA. [3]Department of Mechanical Engineering, University of Colorado, Boulder, CO, USA. [4]Department of Materials Science & Engineering, Iowa State University, Ames, IA, USA. [5]Department of Mechanical & Materials Engineering, Smart Materials and Robotics Lab, University of Nebraska–Lincoln, Lincoln, NE, USA. e-mail: mbartlett@vt.edu

https://doi.org/10.1038/s41563-023-01577-2

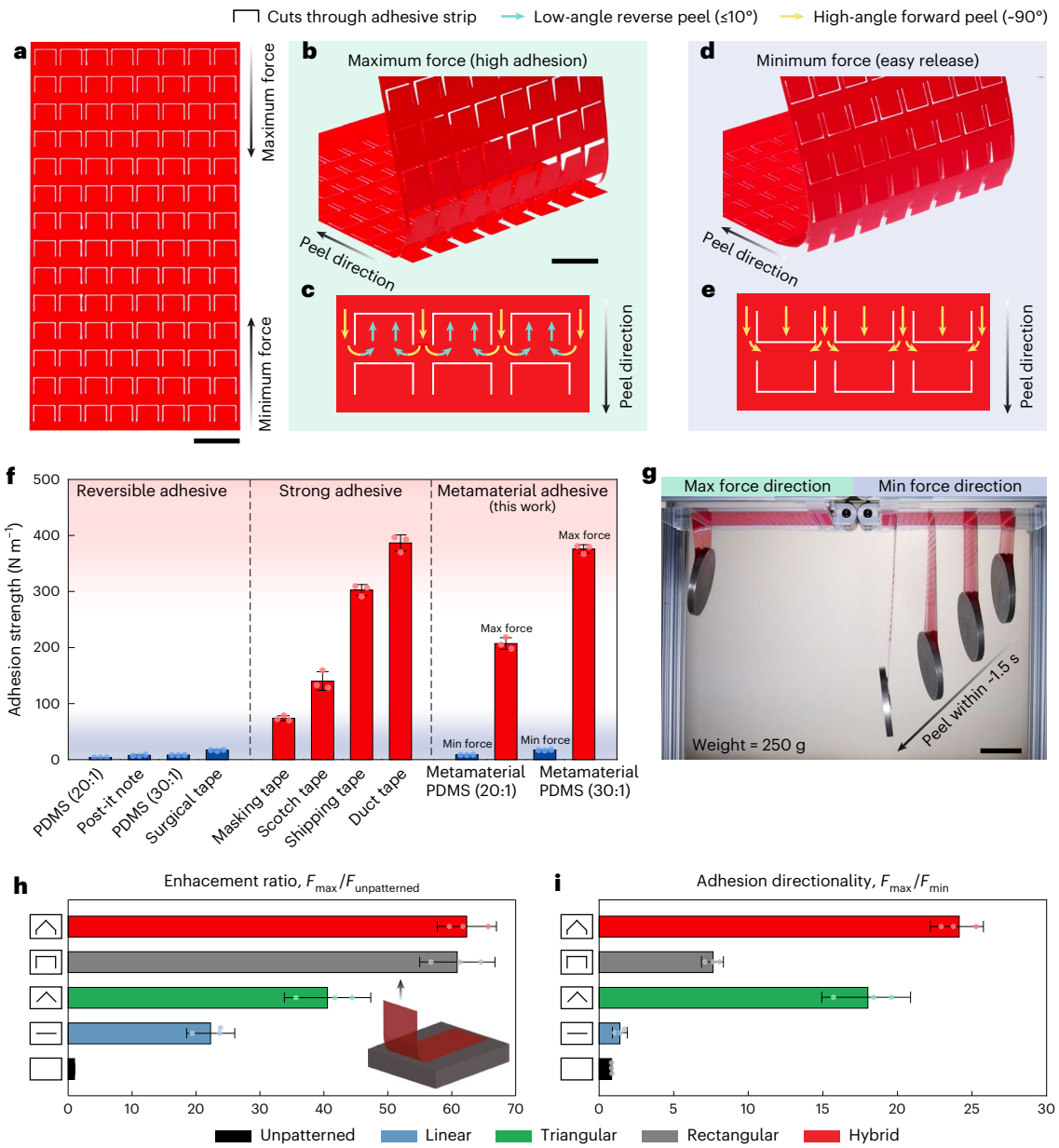

Fig. 1 | High-strength, easy-release metamaterial adhesives. a, The metamaterial adhesive consists of cut patterns in an adhesive film. Scale bar, 15 mm. **b**,**c**, High adhesion is achieved in the maximum force direction (**b**) when cracks propagate at low angles and reverse direction to propagate backwards to separate (**c**). Scale bar, 15 mm. **d**,**e**, Easy release is achieved in the minimum force direction (**d**) as cracks continuously propagate forward to separate (**e**). **f**, Maximum force per total width, or maximum strength, of commercial adhesives and metamaterial adhesives. **g**, A metamaterial adhesive shows high adhesion (maximum force) and easy release (minimum force) in opposite peel directions. Scale bar, 50 mm. **h**, Adhesion enhancement ratios over an unpatterned adhesive for various cut shapes. **i**, Adhesion directionality for various cut shapes. Data are presented as the mean ± s.d. ($n = 3$ measurements from distinct samples for reversible and strong adhesive categories in **f** and from the same sample measured repeatedly for each metamaterial adhesive in **f**, **h** and **i**).

propagation for strong adhesion yet facilitate crack propagation for release and reusability.

Here we introduce a metamaterial adhesive that enables strong and reversible adhesion with directional, spatially selective adhesive strength through programmed nonlinear cut architectures in adhesive films (Fig. 1a). The nonlinear cuts consist of open polygonal shapes that control how adhesive cracks propagate by trapping cracks and then forcing them to reverse direction for high adhesion (Fig. 1b,c), and allow them to propagate forward normally for low adhesion (Fig. 1d,e). Through reverse crack propagation, we decouple high global peel angles into low local peel angles at the adhesive interface. This mechanism enhances adhesion strength up to 60× for strong adhesion relative to the same material without cuts, while also enabling easy release on the order of an unpatterned adhesive by peeling in the opposite direction. These characteristics allow for independent control of adhesion strength and release with reusability. Reverse crack propagation also tunes adhesion strength at any film location and uniquely enables the programming of adhesive strength in two directions simultaneously in a single region of a film. Metamaterial adhesives do not rely on specific chemistry or environmental conditions, microstructured surfaces, or active or patterned stiffness to tune adhesion, but utilize nonlinear cuts for highly systematic control of adhesive crack propagation and direction across a film.

We term these 'metamaterial adhesives' because the nonlinear cut architectures decouple global applied loads into a deterministic local

adhesive response, leveraging insight from mechanical metamaterials, which decouple local and global mechanical properties[36–38]. This functionality is intrinsic to the geometry and allows us to enhance properties and to enable unique adhesion behaviour in a wide range of adhesives, on diverse surfaces, and in dry and wet environments. This applicability to diverse materials allows metamaterial adhesives to leverage both material and geometric mechanisms to span a spectrum of unique adhesive properties, from strong and extremely reversible to extremely strong with reversibility, including adhesives with strengths over 3,000 N m^{-1} (J m^{-2}) that are also reusable and directional. These multifunctional metamaterial adhesives achieve highly systematic control of adhesive crack movement, and this property allows us to achieve an unconventional combination of strong adhesion and easy release, and to programme adhesive strength in two directions simultaneously. This approach has applicability in numerous adhesives, while introducing a digital fabrication framework to automate design and rapidly manufacture adhesives in minutes with deterministic control of adhesive characteristics at any location across a film.

Characteristics of metamaterial adhesives

Our base metamaterial adhesive consists of a polydimethylsiloxane (PDMS) adhesive supported on an inextensible polyethylene terephthalate (PET) backing. Cut architectures are created in a digital design environment and are then rapidly patterned in the adhesive by means of a laser cutter. We define the maximum adhesion force (F_{max}) as the condition at which high adhesion is generated, and the minimum adhesion force (F_{min}) as the condition at which low adhesion or easy release is attained. As adhesive force capacity for an adhesive material is higher at small peel angles[1,39], the selective decoupling of the global and local peel angles provides a mechanism to have a high adhesion in one direction (F_{max}) and easy release in the opposite direction (F_{min}).

Metamaterial adhesives are unique compared to a range of common reversible adhesives and strong adhesives, achieving Post-it Note-like easy release and reusability at F_{min}, with adhesive strength comparable to duct tape at F_{max} (Fig. 1f). This dramatic difference in F_{max} and F_{min} can be observed by hanging a weight on the metamaterial adhesive, where the high strength holds the weight in the maximum force peel direction, yet the metamaterial adhesive releases rapidly in the minimum force peel direction (Fig. 1g and Supplementary Video 1). Adhesion enhancement with easy release is achieved for a variety of nonlinear cut patterns, including triangular, rectangular and hybrid cuts (peel curves in Supplementary Fig. 1). The rectangular and hybrid cuts display an ~60× increase, and triangular cuts an ~40× increase over the unpatterned adhesive, quantified as the enhancement ratio ($F_{max}/F_{unpatterned}$) (Fig. 1h). This adhesion enhancement continues to function over 100 cycles (Supplementary Fig. 2). We quantify the adhesion directionality as F_{max}/F_{min} (Fig. 1i). The hybrid design shows the highest enhancement ratio of ~60× while showing exceptionally easy release with an adhesion directionality of ~25 (details of adhesion metrics are shown in Supplementary Note 1 and Supplementary Fig. 3 and mechanistic schematics are shown in Supplementary Figs. 4 and 5). F_{min} can be tuned by modification of the cut structure into hybrid patterns, detuning of the adhesive layer through laser rastering and adhesive material selection, which enables F_{min} to be equal to or lower than the unpatterned region of the film while maintaining high F_{max} (Supplementary Figs. 6 and 7).

Mechanistic description of reverse crack propagation

To understand the physical origin of the adhesion enhancement and directional release, we quantify the crack propagation behaviour by plotting the crack front velocity versus time during a 90° peel experiment (Fig. 2a). While an unpatterned adhesive separates at a constant, positive velocity (that is, forward), the metamaterial adhesive shows distinct crack dynamics (Supplementary Video 2). Initially, the crack propagates forward through the unpatterned region (zone 1), accelerates as it passes through the interconnects (zone 2) and then is arrested at the base of the rectangular cut where the crack velocity drops to nearly zero and the applied force rises (zone 3). Further loading reverses the crack propagation direction, as indicated by the negative crack velocity, into the adhered rectangular regions at low peel angles (zone 4). In this stage, the local peel angle near the crack tip (α_2) and resultant adhesion force (F) start to increase, resulting in complete adhesive delamination and energy release (Fig. 2b,c). This reverse crack propagation at low angles is only present in the maximum force peeling direction and results in a dramatic rise in adhesive force, as observed in experiments (Fig. 2d and Supplementary Video 3) and captured in simulations using finite-element analysis (FEA) (Fig. 2e, Supplementary Note 2 and Supplementary Fig. 8). In the minimum force peel direction and in unpatterned adhesives the crack only propagates forward at low forces, as commonly observed in adhesive debonding. Linear cut patterns and closed-polygonal-shaped incisions only show primarily forward or lateral crack propagation[30,32], not systematic reverse crack propagation, which gives metamaterial adhesives superior enhancement, directionality and spatial control of adhesion.

The cut size is critical for achieving optimized adhesion enhancement. When the width w_p of rectangular cuts is varied with other dimensions fixed, the adhesion force per cut pattern, F_{max}/N_p, first increases with w_p and then saturates when $0.5w_p$ exceeds a critical value (Fig. 2f). The underlying mechanism is the transition between two distinct regimes of reverse crack propagation. When $0.5w_p$ exceeds a characteristic length l_{ch}, cracks originating at the tips of interconnects do not interfere with each other, leading to circular delaminated regions centred at each interconnect (Fig. 2g and Supplementary Fig. 9a). When $0.5w_p$ is smaller than l_{ch}, cracks from neighbouring interconnect tips merge before F_{max} is reached, resulting in an approximately uniform crack front during reverse crack propagation (Fig. 2h and Supplementary Fig. 9b). Theoretical analysis yields (Supplementary Note 3):

$$l_{ch} = \sqrt{\frac{2D}{G_c}\frac{w_{int}}{w}(N_p^* + 1)} \quad (1)$$

where D is the flexural rigidity of the adhesive film, w_{int} is the width of an interconnect, N_p^* is the optimal number of cut patterns that results in the highest F_{max}, w is the total width and G_c is the critical energy release rate. Whereas D, w_{int}, w and G_c are prescribed parameters, N_p^* can be either determined experimentally or solved algebraically (Supplementary Note 3). Theoretical analysis also shows that F_{max} is maximized when $0.5w_p = l_{ch}$ (Supplementary Note 3), making l_{ch} a key length for cut design.

Applicability in diverse materials, surfaces and environments

To evaluate the versatility of the characteristic length l_{ch}, we applied rectangular cuts with different width w_p to various sets of adhesives, including PET/PDMS and commercial adhesives such as 3M Post-it Note, 3M CoTran backing film/Dow Corning MG-7 9900 Soft Skin Adhesive and 3M Micropore. For each adhesive, the l_{ch} calculated using the theoretically solved N_p^* (Supplementary Note 3) agrees well with the experimentally determined N_p^* (Supplementary Table 1). In Fig. 3a the normalized maximum adhesive forces for all of these different adhesives collapse onto a single master curve normalized by l_{ch}. This demonstrates that the metamaterial adhesive design approach is widely applicable to diverse materials and must be systematically designed around l_{ch}. Furthermore, other in-plane dimensions (spacing s, cut length l_p) must also be equal to or greater than l_{ch}. This avoids the premature interaction of adhesive cracks and allows for full adhesion enhancement (Supplementary Figs. 9–11), providing general guidance for metamaterial adhesive design.

The metamaterial adhesive strategy is applicable to diverse substrates and conditions. When we applied and measured the adhesive underwater, water is displaced and adhesion is enhanced (at least 30×

https://doi.org/10.1038/s41563-023-01577-2

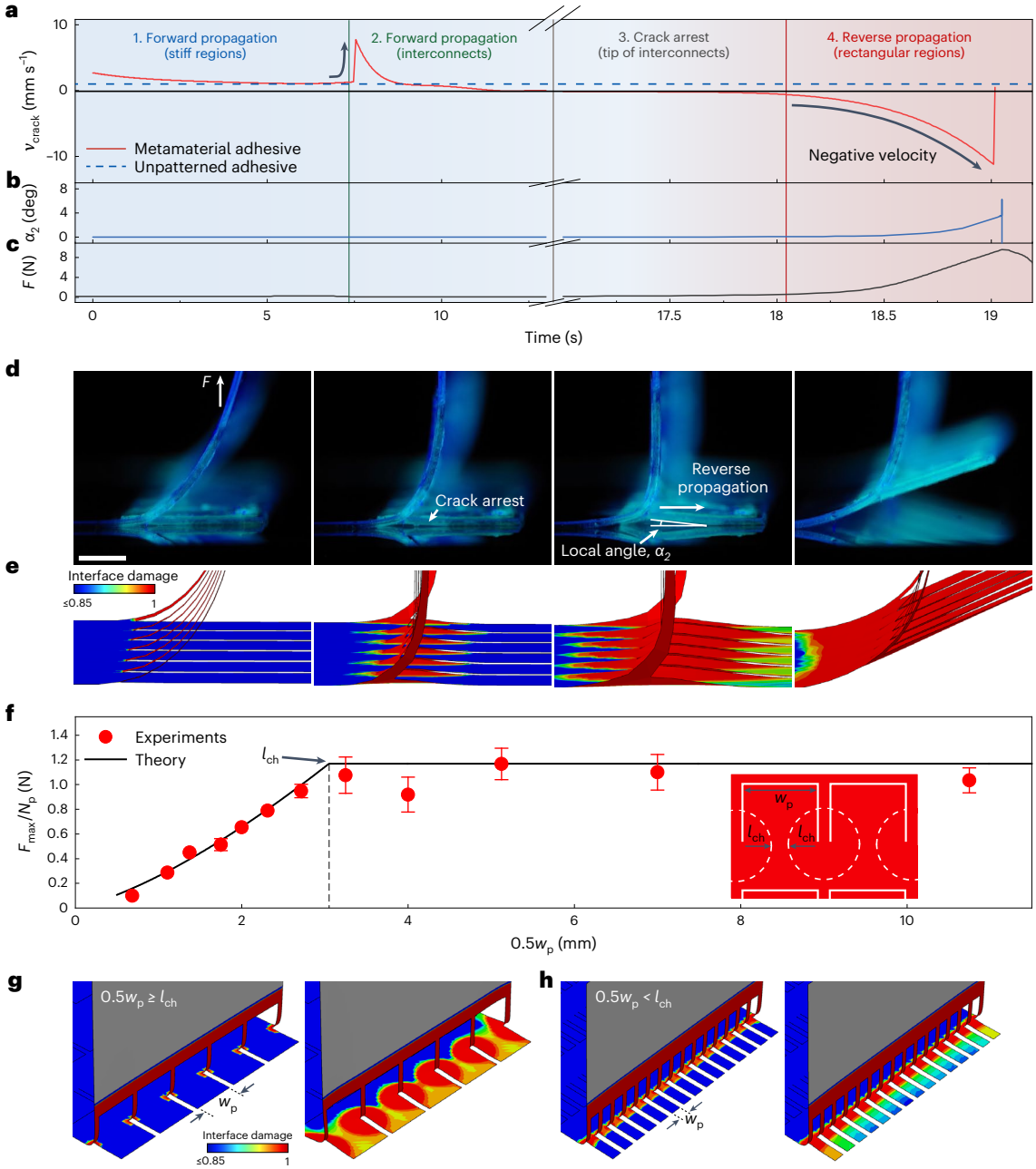

Fig. 2 | Enhancing adhesion through reverse crack propagation. a, Crack velocity versus time for a metamaterial adhesive and unpatterned adhesive. **b**, Local peel angle near the crack tip from FEA. **c**, Measured force versus time of the metamaterial adhesive. **d**,**e**, Side profile images of a peeling adhesive (scale bar, 2 mm) (**d**), and corresponding FEA results (**e**). **f**, Maximum force per cut pattern F_{max}/N_p versus half cut width $0.5w_p$. Solid line is the theoretical fit (Supplementary Note 3). **g**,**h**, FEA results showing crack arrest at interconnect tips (left) and crack morphology at $F = F_{max}$ (right) for $0.5w_p \geq l_{ch}$ (**g**) and $0.5w_p < l_{ch}$ (**h**). The colour contours in **e**, **g** and **h** illustrate the interface damage, which ranges from 0 (fully adhered) to 1 (completely delaminated). Data in **f** are presented as mean ± s.d. ($n = 3$ measurements from the same sample measured repeatedly).

and up to 56×) relative to unpatterned adhesives on glass, plastic/PMMA, aluminium, steel and Teflon (Fig. 3b and Supplementary Figs. 12 and 13). These results validate that metamaterial adhesives are applicable over a wide range of material types, substrates and environments to enhance adhesion without specific chemistry or surface topology.

Performance of metamaterial adhesives

The adhesion performance of metamaterial adhesives is highlighted by comparing combinations of adhesion enhancement, directionality and strength to previous literature results (Fig. 3c,d). Here we compare the metamaterial adhesives to hydrogels[13,40–44], chemical patterns[12,45,46], stiffness patterns[3,23,30–32,47] and bioinspired patterns[2,15,18,35,48–50]. Figure 3c shows that adhesives commonly show enhancement with little directionality (blue shaded region), or directionality with little enhancement (green shaded region), whereas metamaterial adhesives can be made with both high enhancement and directionality (red shaded region). Figure 3d shows that directional adhesives typically show low strength (green shaded region) whereas high-strength adhesives (blue shaded region) show little directionality. Metamaterial adhesives overcome these challenges and show unique adhesive properties, from strong and extremely directional (top-left quadrant) to extremely strong with directionality (bottom-right quadrant) while being reusable in

https://doi.org/10.1038/s41563-023-01577-2

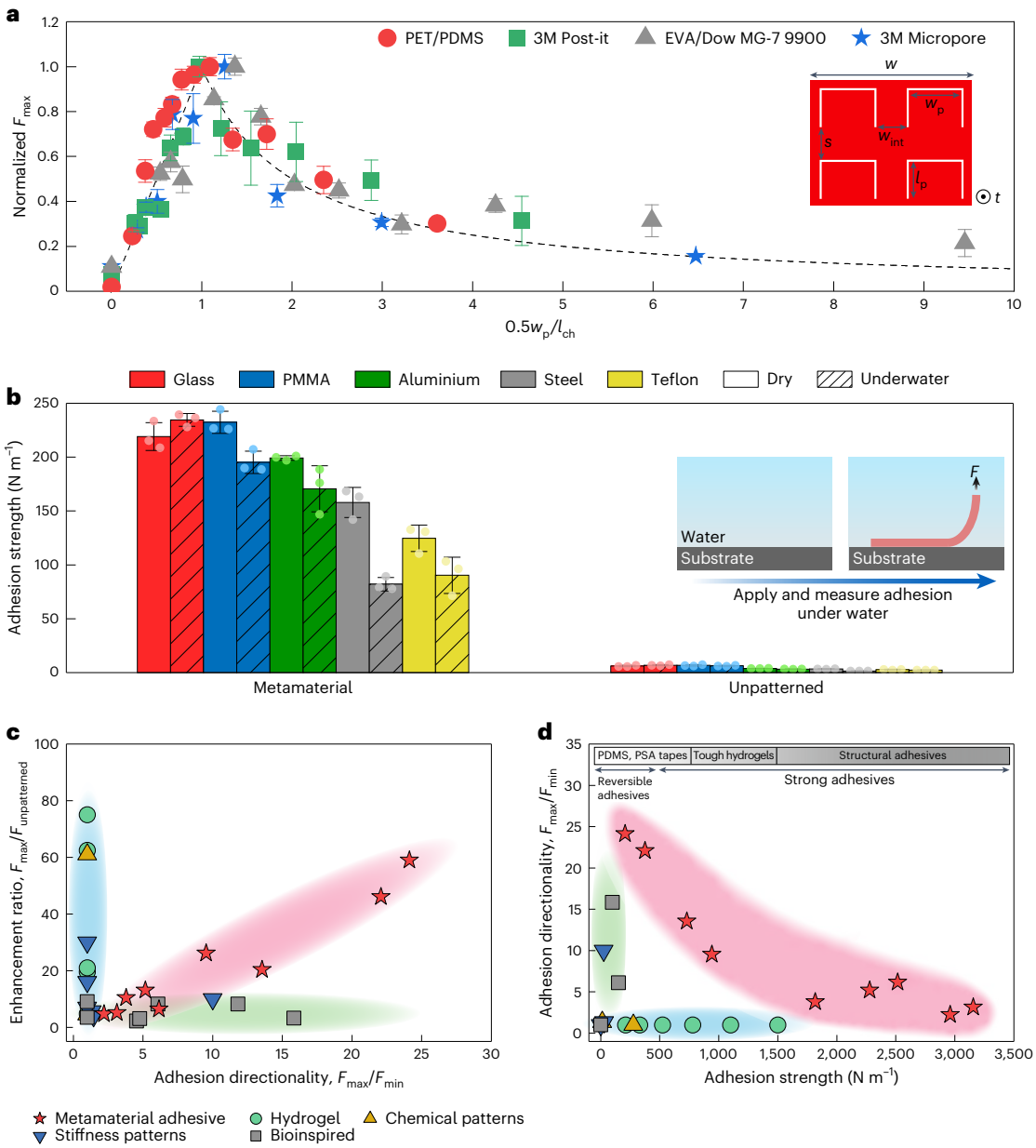

Fig. 3 | Versatility and performance comparisons of metamaterial adhesives. **a**, Normalized maximum adhesion versus $0.5w_p/l_{ch}$ for different metamaterial adhesive materials; the dashed line indicates a single master curve where experimental data points collapse. **b**, Maximum force per width of metamaterial adhesives versus unpatterned adhesives on diverse surfaces in dry and underwater environments. **c**,**d**, Comparison plots of enhancement ratio versus adhesion directionality (**c**) and adhesion directionality versus adhesion strength (**d**) show that metamaterial adhesives occupy unique regions of the adhesive property space. This comparison is for passive adhesives (that is, no trigger release), no kinetic control (that is, not comparing low to high testing rates), and on nominally smooth surfaces. See Supplementary Fig. 14 and Supplementary Table 2 for detailed identification of data points. Data in **a** and **b** are presented as mean ± s.d. ($n = 3$ measurements from the same sample measured repeatedly).

all cases (red shaded region). This includes metamaterial adhesives with intrinsically strong acrylic adhesive layers such as 3M VHB (Very High Bond). This enhanced adhesion beyond the already strong unpatterned adhesive and increased strength (which is equivalent to adhesion toughness for 90° peeling) to over 3,000 N m^{-1} (J m^{-2}). Notably, these very strong metamaterial adhesives were still directional and were reusable over multiple testing cycles (see Supplementary Fig. 2 for cyclic data), which is uncommon because strong adhesives typically rely on bonding mechanisms which are not directional and do not function beyond a single cycle. These types of properties demonstrate the versatility of metamaterial adhesives and open exciting performance characteristics for adhesive materials.

Digital manufacturing and design of metamaterial adhesives

Metamaterial adhesives can enable spatial tunability of adhesion. We utilize digital fabrication with computer-aided design and laser-based subtractive manufacturing to enable rapid, maskless fabrication of programmed adhesion profiles (Fig. 4a). As a demonstration, we design adhesives with rectangular cut patterns in the shape of the letters, "HELLO" (Supplementary Fig. 15). Lower adhesion can also be achieved by locally reducing width, allowing for adhesive force contrast ratios of over 320× (Supplementary Fig. 16). With selectable adhesion at specific locations, we can go further to design spatially anisotropic adhesion, where a specific region can be programmed to have a prescribed adhesive strength in two directions simultaneously.

https://doi.org/10.1038/s41563-023-01577-2

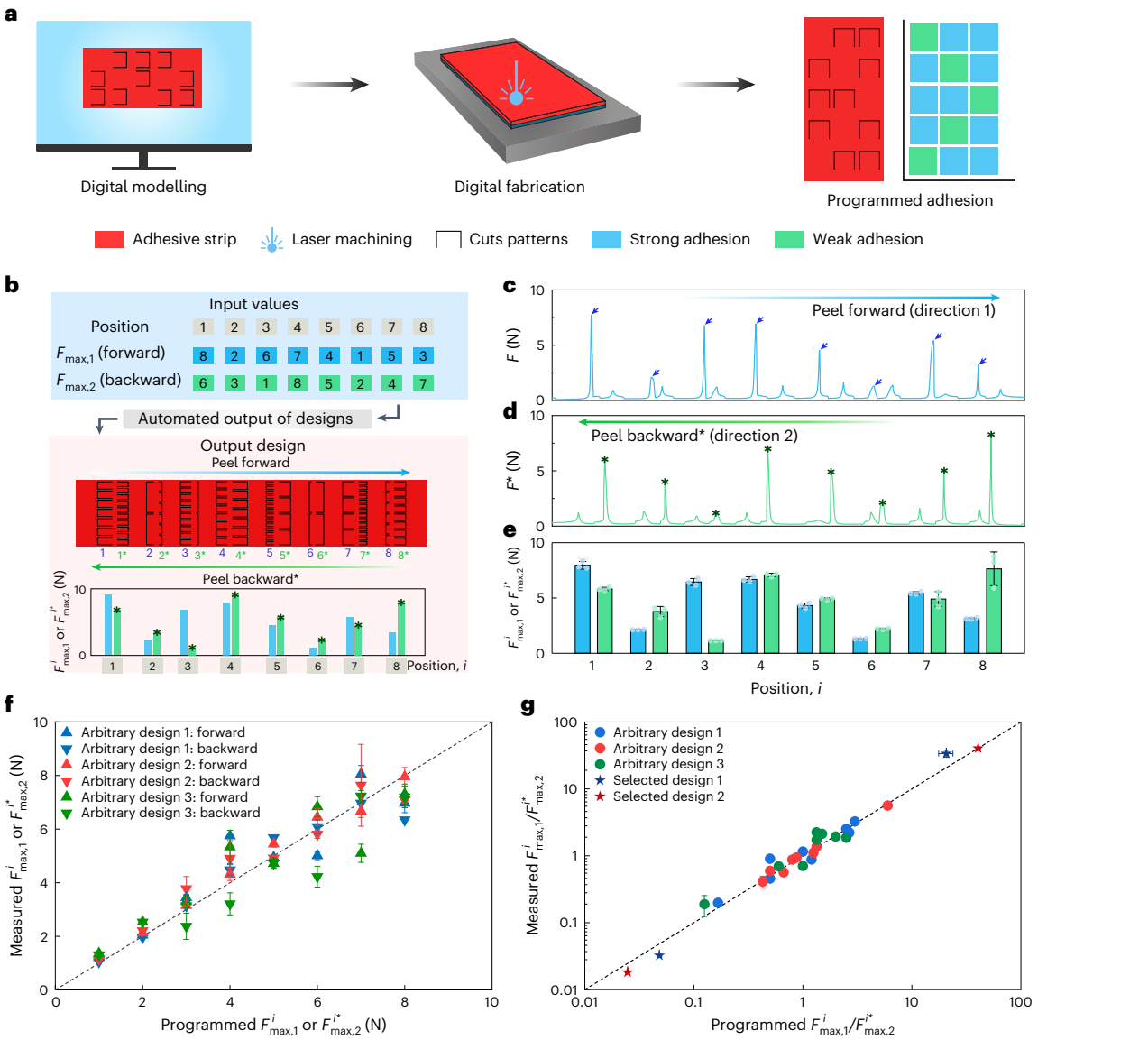

Fig. 4 | Digitalized adhesive fabrication. a, Digital fabrication scheme for programmable metamaterial adhesives. **b**, Automated design generates a layout of programmed adhesion strength represented by the output design. **c**–**e**, Force versus position for the adhesive fabricated with the automated design in Fig. 4b in the forward direction (**c**) and in the backward direction (**d**), and compiled data as a function of position (**e**). **f**, Measured and programmed maximum forces show excellent agreement. **g**, Decoupling of directionality, which creates maximum/maximum forces at each region in both forward/backward directions, shows good agreement with programmed and measured results for both arbitrary and selected designs. Data in **e**–**g** are presented as mean ± s.d. ($n = 3$ measurements from the same sample measured repeatedly).

We spatially programmed adhesion in discrete regions and decoupled the directionality by introducing a second set of rectangular cuts into each adhesive region to independently tune the maximum force in both peel directions (Fig. 4b–e). We can also automate design where the user selects a desired F_{max} in the forward direction ($F_{max,1}$) and backward direction ($F_{max,2}$) for a specific location; then an inverse design algorithm automates a cut pattern and a laser cutter file is generated.

The programmed and experimental adhesion data show strong agreement for three different arbitrary designs, highlighting the ability to reliably create customized, spatially controlled adhesion (Fig. 4f). We next plot the bidirectional enhancement ratios ($F^i_{max,1}/F^{i*}_{max,2}$, where i is the location index) of each region in Fig. 4g. We find good agreement between measured and programmed force ratios for the arbitrarily generated designs and two selected designs to maximize the range of the bidirectional enhancement ratios (Supplementary Fig. 17). This enables a range of 0.018–41, a difference of over three orders of magnitude (~2,300×), showing tremendous ability to programme adhesion force in two directions simultaneously at a single region of a film. Chemical and microscale patterns and linear cut features may be able to spatially control adhesion by pinning cracks, but are unable to readily control directional adhesive strength at specific locations as we demonstrate with metamaterial adhesives and our digital fabrication approach.

Demonstrations of metamaterial adhesives

High-adhesion yet easy-release capabilities are critical for numerous applications. To demonstrate metamaterial adhesives in packaging, we added a layout of cut patterns into a commercial shipping tape, such that strong bonding ensures sealing in all directions yet the adhesive can be removed on demand by peeling in a particular direction (Fig. 5a). A box sealed with metamaterial tape withstood the weight and impact of a brick (1,550 g) over five drop impacts, while the box sealed with the same tape without metamaterial cuts completely collapsed only after

https://doi.org/10.1038/s41563-023-01577-2

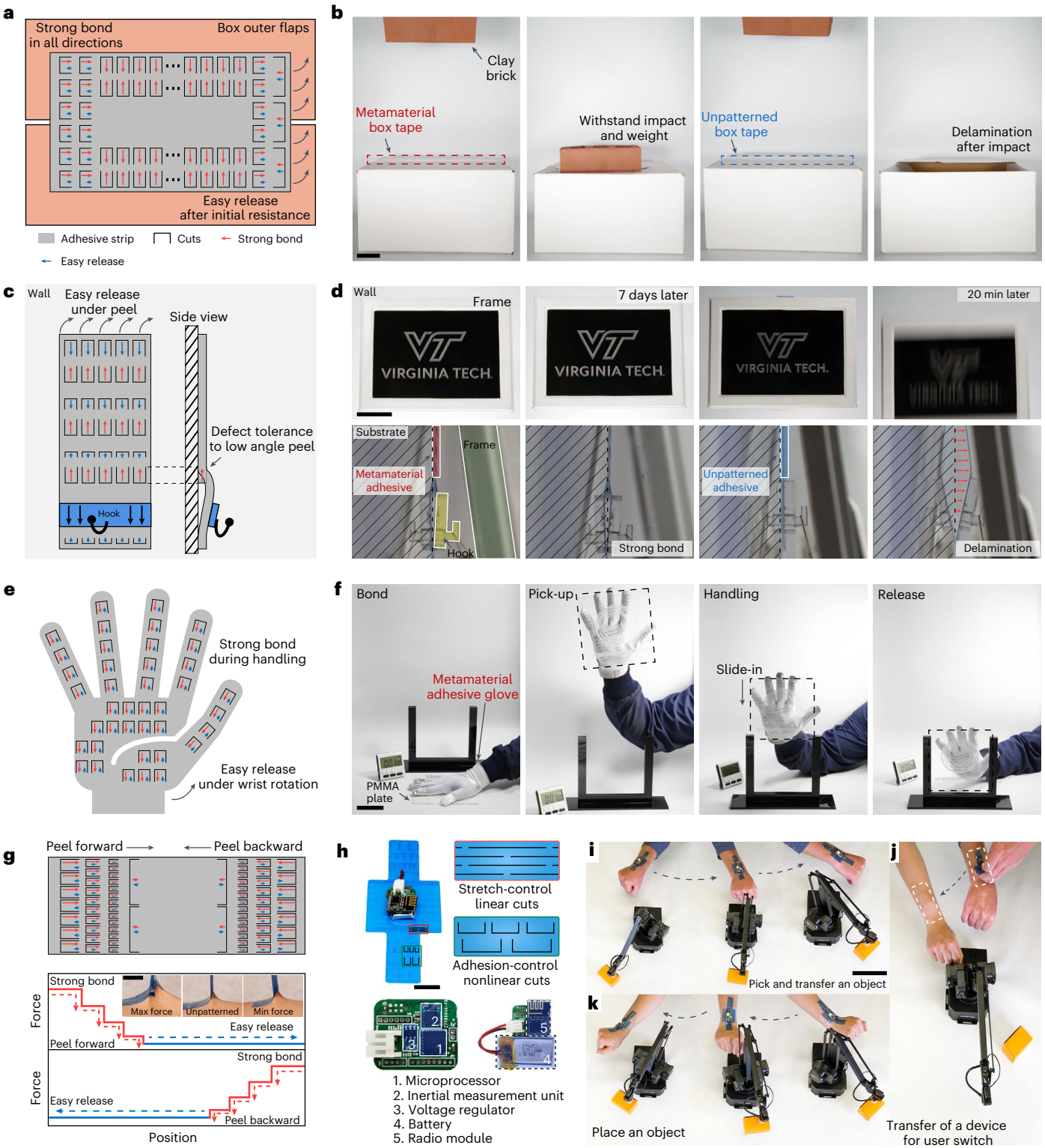

Fig. 5 | Metamaterial adhesives with programmable strength and direction. **a**, Metamaterial adhesive box tape design. **b**, A metamaterial adhesive made of box tape holds a box closed during impact of a brick, whereas a pristine box tape delaminates and fails. Scale bar, 50 mm. **c**, Metamaterial adhesive wall hanging design. **d**, A metamaterial adhesive supports a frame for over 7 days and is then easily removed, whereas a pristine adhesive fails after 20 min. Scale bar, 50 mm. **e**, Metamaterial adhesive glove design. **f**, A metamaterial adhesive glove can pick up flat, fragile objects, transport these to a desired area, and then release the object easily. Scale bar, 100 mm. **g**, Metamaterial adhesive wearable patch design. Scale bar, 15 mm. **h**, A wireless wearable motion control device. Scale bar, 15 mm. **i**, An object is picked and transported by a robotic arm controlled by the device adhered to a user's arm. Scale bar, 100 mm. **j**, The device is transferred to another user's arm. **k**, The object is transported and released. Registered Virginia Tech trademark printed with the approval of Virginia Tech Office of Licensing and Trademarks.

two drops (Fig. 5a,b and Supplementary Video 4). The metamaterial adhesive can also hang objects on a wall, while still being easily removed (Fig. 5c). Furthermore, we used the ability to control adhesion strength in two directions at one location to make the hanging more robust, where adhesion strength was increased at the top and bottom edges to prevent inadvertent release. A frame hung on a wall with a metamaterial adhesive remained in place for over 7 days without any observed delamination and was then easily released (Supplementary Video 5), while the frame supported by an unpatterned adhesive fell off within 20 min (Fig. 5d). Metamaterial adhesives can also be applied in wearable form factors. A metamaterial adhesive pick-and-release glove was created by laser-machining nonlinear cuts into an elastomer-coated glove. This allowed a user to pick up a flat object, hold it reliably and then effortlessly release the object into a predetermineded location through wrist rotation, while the unpatterned glove dropped the object (Fig. 5e,f and Supplementary Video 6).

A metamaterial adhesive strip was also created for a human-in-the-loop wearable device (Fig. 5h). Here the metamaterial adhesive had high adhesion at the edges for strong attachment with easy removal after initial peeling, which was qualitatively observed through substantial skin deformation in the F_{max} direction, relative to the unpatterned and F_{min} direction (Fig. 5g). The wearable device, which captures human motion and wirelessly transmits the signal to a mirrored robotic arm, was attached to the arm of a first user where an object was picked, displaced and released from the robotic arm (Fig. 5i and Supplementary Video 7), and then transferred to another user to move the object again (Fig. 5j,k). Cut patterns can also be extended to a variety of adhesive patch shapes, including a circular adhesive patch for a wearable physiological monitoring device (Supplementary Fig. 18).

Discussion

Our metamaterial adhesive strategy functions with a range of adhesives on diverse substrates and conditions to enhance adhesion, provide directionality and spatially programme adhesive strength across an adhesive sheet in multiple directions simultaneously. Through a maskless, digital fabrication environment, we can rapidly output diverse adhesive characteristics that cannot be done with chemical or microfeature patterns. Additionally, millimetre–centimetre scale cuts could be created with roll-to-roll techniques such as rotary die cutting, providing avenues for scale-up. Although our metamaterial adhesive approach works in diverse materials, the cuts introduce locations for possible rupture, and backings that are meant to tear could exacerbate this effect. However, the cut features may also improve tearability, which might be useful for counterfeit protection and easy dispensing of tapes. Our reverse crack propagation mechanism for programmable adhesion may also enable new opportunities in other fracture processes, such as toughening bulk materials, adhesion control in micro/nano systems (see Supplementary Fig. 19 for dimensional scaling predictions) and adhesion for locomotion in robotics. Thus, these metamaterial adhesives can serve as the foundation for the exceptional control of adhesion in diverse materials and applications.

Online content

Any methods, additional references, Nature Portfolio reporting summaries, source data, extended data, supplementary information, acknowledgements, peer review information; details of author contributions and competing interests; and statements of data and code availability are available at https://doi.org/10.1038/s41563-023-01577-2.

References

1. Kinloch, A. J. *Adhesion and Adhesives: Science and Technology* (Springer, 2012).
2. Glassmaker, N. J., Jagota, A., Hui, C.-Y., Noderer, W. L. & Chaudhury, M. K. Biologically inspired crack trapping for enhanced adhesion. *Proc. Natl Acad. Sci. USA* **104**, 10786–10791 (2007).
3. Majumder, A., Ghatak, A. & Sharma, A. Microfluidic adhesion induced by subsurface microstructures. *Science* **318**, 258–261 (2007).
4. Creton, C. & Ciccotti, M. Fracture and adhesion of soft materials: a review. *Reports Prog. Phys.* **79**, 046601 (2016).
5. Hwang, I. et al. Multifunctional smart skin adhesive patches for advanced health care. *Adv. Healthc. Mater.* **7**, 1800275 (2018).
6. Dickey, M. D. Stretchable and soft electronics using liquid metals. *Adv. Mater.* **29**, 1606425 (2017).
7. Packham, D. E. Adhesive technology and sustainability. *Int. J. Adhes. Adhes.* **29**, 248–252 (2009).
8. Chu, B., Jung, K., Han, C. S. & Hong, D. A survey of climbing robots: locomotion and adhesion. *Int. J. Precis. Eng. Manuf.* **11**, 633–647 (2010).
9. Kim, S. et al. Microstructured elastomeric surfaces with reversible adhesion and examples of their use in deterministic assembly by transfer printing. *Proc. Natl Acad. Sci. USA* **107**, 17095–17100 (2010).
10. Graule, M. A. et al. Perching and takeoff of a robotic insect on overhangs using switchable electrostatic adhesion. *Science* **352**, 978–982 (2016).
11. Lee, H., Lee, B. P. & Messersmith, P. B. A reversible wet/dry adhesive inspired by mussels and geckos. *Nature* **448**, 338–341 (2007).
12. Xia, S., Ponson, L., Ravichandran, G. & Bhattacharya, K. Adhesion of heterogeneous thin films II: adhesive heterogeneity. *J. Mech. Phys. Solids* **83**, 88–103 (2015).
13. Yuk, H. et al. Dry double-sided tape for adhesion of wet tissues and devices. *Nature* **575**, 169–174 (2019).
14. Yang, J., Bai, R., Chen, B. & Suo, Z. Hydrogel adhesion: a supramolecular synergy of chemistry, topology, and mechanics. *Adv. Func. Mater.* **30**, 1901693 (2020).
15. Qu, L., Dai, L., Stone, M., Xia, Z. & Wang, Z. L. Carbon nanotube arrays with strong shear binding-on and easy normal lifting-off. *Science* **322**, 238–242 (2008).
16. Boesel, L. F., Greiner, C., Arzt, E. & Del Campo, A. Gecko-inspired surfaces: a path to strong and reversible dry adhesives. *Adv. Mater.* **22**, 2125–2137 (2010).
17. Chan, E. P., Smith, E. J., Hayward, R. C. & Crosby, A. J. Surface wrinkles for smart adhesion. *Adv. Mater.* **20**, 711–716 (2008).
18. Baik, S. et al. A wet-tolerant adhesive patch inspired by protuberances in suction cups of octopi. *Nature* **546**, 396–400 (2017).
19. Drotlef, D.-M., Amjadi, M., Yunusa, M. & Sitti, M. Bioinspired composite microfibers for skin adhesion and signal amplification of wearable sensors. *Adv. Mater.* **29**, 1701353 (2017).
20. Yu, J. et al. Gecko-inspired dry adhesive for robotic applications. *Adv. Func. Mater.* **21**, 3010–3018 (2011).
21. Kwak, M. K., Jeong, H. E. & Suh, K. Y. Rational design and enhanced biocompatibility of a dry adhesive medical skin patch. *Adv. Mater.* **23**, 3949–3953 (2011).
22. Kendall, K. Control of cracks by interfaces in composites. *Proc. R. Soc. A* **341**, 409–428 (1975).
23. Xia, S., Ponson, L., Ravichandran, G. & Bhattacharya, K. Toughening and asymmetry in peeling of heterogeneous adhesives. *Phys. Rev. Lett.* **108**, 196101 (2012).
24. Xia, S., Ponson, L., Ravichandran, G. & Bhattacharya, K. Adhesion of heterogeneous thin films—I: elastic heterogeneity. *J. Mech. Phys. Solids* **61**, 838–851 (2013).
25. Ghareeb, A. & Elbanna, A. Extreme enhancement of interfacial adhesion by bulk patterning of sacrificial cuts. *Extreme Mech. Lett.* **28**, 22–30 (2019).
26. Croll, A. B., Hosseini, N. & Bartlett, M. D. Switchable adhesives for multifunctional interfaces. *Adv. Mater. Technol.* **4**, 1900193 (2019).
27. Haverkamp, C. B., Hwang, D., Lee, C. & Bartlett, M. D. Deterministic control of adhesive crack propagation through jamming based switchable adhesives. *Soft Matter* **17**, 1731–1737 (2021).

28. Akulichev, A., Tiwari, A., Dorogin, L., Echtermeyer, A. & Persson, B. Rubber adhesion below the glass transition temperature: role of frozen-in elastic deformation. *Europhys. Lett.* **120**, 36002 (2018).
29. Cho, H. et al. Intrinsically reversible superglues via shape adaptation inspired by snail epiphragm. *Proc. Natl Acad. Sci. USA* **116**, 13774–13779 (2019).
30. Chung, J. Y. & Chaudhury, M. K. Roles of discontinuities in bio-inspired adhesive pads. *J. R. Soc. Interface* **2**, 55–61 (2005).
31. Ghatak, A., Mahadevan, L., Chung, J. Y., Chaudhury, M. K. & Shenoy, V. Peeling from a biomimetically patterned thin elastic film. *Proc. R. Soc. Lond. A* **460**, 2725–2735 (2004).
32. Hwang, D. G., Trent, K. & Bartlett, M. D. Kirigami-inspired structures for smart adhesion. *ACS Appl. Mater. Interfaces* **10**, 6747–6754 (2018).
33. Zhao, R., Lin, S., Yuk, H. & Zhao, X. Kirigami enhances film adhesion. *Soft Matter* **14**, 2515–2525 (2018).
34. Wang, H., Pan, C., Zhao, H., Wang, T. & Han, Y. Design of a metamaterial film with excellent conformability and adhesion for bandage substrates. *J. Mech. Behav. Biomed. Mater.* **124**, 104799 (2021).
35. Jeong, H. E., Lee, J.-K., Kim, H. N., Moon, S. H. & Suh, K. Y. A nontransferring dry adhesive with hierarchical polymer nanohairs. *Proc. Natl Acad. Sci. USA* **106**, 5639–5644 (2009).
36. Overvelde, J. T. B., Weaver, J. C., Hoberman, C. & Bertoldi, K. Rational design of reconfigurable prismatic architected materials. *Nature* **541**, 347–352 (2017).
37. Holmes, D. P. Elasticity and stability of shape changing structures. *Curr. Opin. Colloid Interface Sci.* **40**, 118–137 (2019).
38. Chen, T., Pauly, M. & Reis, P. M. A reprogrammable mechanical metamaterial with stable memory. *Nature* **589**, 386–390 (2021).
39. Kendall, K. Thin-film peeling—the elastic term. *J. Phys. D* **8**, 1449–1452 (1975).
40. Steck, J., Kim, J., Yang, J., Hassan, S. & Suo, Z. Topological adhesion. I. rapid and strong topohesives. *Extreme Mech. Lett.* **39**, 100803 (2020).
41. Liu, X., Zhang, Q., Gao, Z., Hou, R. & Gao, G. Bioinspired adhesive hydrogel driven by adenine and thymine. *ACS Appl. Mater. Interfaces* **9**, 17645–17652 (2017).
42. Li, J. et al. Tough adhesives for diverse wet surfaces. *Science* **357**, 378–381 (2017).
43. Liu, X., Zhang, Q. & Gao, G. Bioinspired adhesive hydrogels tackified by nucleobases. *Adv. Func. Mater.* **27**, 1703132 (2017).
44. Yuk, H., Zhang, T., Lin, S., Parada, G. A. & Zhao, X. Tough bonding of hydrogels to diverse non-porous surfaces. *Nat. Mater.* **15**, 190–196 (2016).
45. Chan, E. P., Ahn, D. & Crosby, A. J. Adhesion of patterned reactive interfaces. *J. Adhes.* **83**, 473–489 (2007).
46. Ramrus, D. A. & Berg, J. C. Enhancement of adhesion to heterogeneously patterned substrates. *Colloids Surf. A* **273**, 84–89 (2006).
47. Ghareeb, A. & Elbanna, A. Adhesion asymmetry in peeling of thin films with homogeneous material properties: a geometry-inspired design paradigm. *J. Appl. Mech.* **86**, 071005 (2019).
48. Sameoto, D., Sharif, H., Díaz Téllez, J. P., Ferguson, B. & Menon, C. Nonangled anisotropic elastomeric dry adhesives with tailorable normal adhesion strength and high directionality. *J. Adhes. Sci. Technol.* **28**, 354–366 (2014).
49. Kwak, M. K., Jeong, H. E., Bae, W. G., Jung, H.-S. & Suh, K. Y. Anisotropic adhesion properties of triangular-tip-shaped micropillars. *Small* **7**, 2296–2300 (2011).
50. Kim, T., Jeong, H. E., Suh, K. Y. & Lee, H. H. Stooped nanohairs: geometry-controllable, unidirectional, reversible, and robust gecko-like dry adhesive. *Adv. Mater.* **21**, 2276–2281 (2009).

Methods

Materials

Adhesive films were made with silicone adhesives (Sylgard 184, MG-7 1010 and 9900 Soft Skin Adhesive; Dow Corning), or polyurethane adhesives (Vytaflex 30; Smooth-On) and backing layers (PET; Grainger and CoTran pigmented polyethylene monolayer backing film 9718; 3M, thickness (t_b) ≈ 100 μm). We used commercial Post-it Notes (3M) and Micropore medical surgical tapes (3M) for adhesive fabrication with cut patterns. For adhesion tests that compare commercial adhesives with metamaterial adhesives, we used commercial Post-it Notes, Micropore medical surgical tapes, 101+ masking tape (3M), Scotch Magic Greener tape (3M), Scotch heavy-duty shipping packaging tape (3M) and Scotch multipurpose waterproof duct tape 3960-RD (3M). The G_c values for all commercial adhesives were measured using the same conditions as metamaterial adhesives, using a 90° peel set-up at 1 mm s^{-1}. For adhesion tests on multiple substrates, we used cast PMMA sheet, borosilicate glass sheet, multipurpose 304 stainless steel bar, multipurpose 6061 aluminium bar and Teflon PTFE bar (McMaster-Carr). For colouring samples, we used Silc-Pig pigments and Ignite fluorescent pigments (Smooth-On).

Adhesive preparation

Adhesives were composed of a PET backing layer and a PDMS adhesive layer. A thin PDMS elastomeric layer (20:1 base resin-to-crosslinker ratio; elastic modulus (E) = 880 ± 40 kPa, t_{PDMS} ≈ 120 μm or 30:1 base resin-to-crosslinker ratio; E = 86 ± 9 kPa, t_{PDMS} ≈ 120 μm) was created on a glass plate using a thin film applicator (ZUA 2000; Zehntner Testing Instruments) and cured at 80 °C for 60 min. PET films (E = 2.6 ± 0.1 GPa) were treated with oxygen plasma (3 min, 300 mtorr oxygen, 400 W; PE-75 Series, Plasma Etch), and another layer of PDMS with the same mixing ratio was cast onto the cured PDMS layer using a thin film applicator (t_{PDMS} ≈ 30 μm). The surface-treated PET films were placed on the uncured PDMS layer, and the adhesive composite was cured in the oven at 80 °C for 60 min. For 20:1 PDMS adhesives, t_{PET} = 75 μm. For 30:1 PDMS adhesives, t_{PET} = 125 μm for Fig. 1f and t_{PET} = 75 μm for Fig. 3b. The adhesive composite was then patterned using a laser machine (Epilog Laser Fusion M2, 75 W). VHB adhesives were composed of a PET backing layer and a VHB adhesive layer. PET films were treated with oxygen plasma (3 min, 300 mtorr oxygen, 400 W; PE-75 Series). A VHB layer (75 or 125 μm) was applied onto the surface-treated PET films using a seam roller (Seam Rollers). For the demonstration of a hanging frame, the adhesives were fabricated with polyurethane elastomers.

Adhesion tests

A 90° peel test set-up was utilized to measure the adhesion strength between an adhesive strip and an acrylic substrate on an Instron 5944 mechanical tester with Bluehill 3 software at a constant displacement rate of 1 mm s^{-1}. Before each run, the adhesive surface of each PDMS specimen was cleaned with isopropyl alcohol. For each specific condition, the same sample was measured repeatedly, except for the commercial adhesives in Fig. 1, where distinct samples were measured. The adhesive strip was placed on an acrylic substrate and applied with a rubber roller with a dwell time of 3 min before executing a test. For the underwater test, the adhesive was first immersed in the water for 5 min before being attached to each substrate and was tested with a dwell time of 3 min. Data obtained from all adhesive tests were analysed in MATLAB (R2020a). The critical energy release rate G_c of an adhesive strip was calculated by averaging the steady-state adhesion data points obtained from an unpatterned adhesive strip. For the crack analysis, we recorded video during the peel test and the video was analysed with a video analysis tool (Tracker v.5.1.5, Open Source Physics).

Adhesion simulations

FEA for the peeling mechanics of metamaterial adhesives was conducted using ABAQUS software (v.2020). Further details are given in Supplementary Note 2.

Fabrication of the human–robot interface and biomonitoring patch

A silicone adhesive (MG-7 1010 Soft Skin Adhesive; Dow Corning) and a PET layer (t_{PET} = 50 μm) were used to create adhesive patches by following the same fabrication procedures above. For both demonstrations, the wearable electronics were integrated with the metamaterial adhesive using a silicone adhesive (Sil-poxy; Smooth-On). For the human motion control sensor, the electronics were composed of a microcontroller (STM32; STMicroelectronics), inertia measurement unit (ICM-20948; InvenSense TDK), radiofrequency transceiver (nRF24L01+; Nordic) and a rechargeable battery with power regulation. The pose of the human arm was estimated by integrating the signal from the three-axis gyroscope. The rotation signal was recorded using an on-board microcontroller, then wirelessly transmitted to another microcontroller that was used to control the robotic arm (uArm Swift Pro; UFACTORY). Once the robotic arm reached the vicinity of a desired location, a preprogrammed sequence of commands was executed to pick, displace and release an object at a different location. A wearable pulse oximeter (MAX30101, Maxim) was wired to a microcontroller (STM32; STMicroelectronics) using a flexible printed circuit board for signal processing and recording. The recorded signals were normalized and filtered using a low-pass filter.

Reporting summary

Further information on research design is available in the Nature Portfolio Reporting Summary linked to this article.

Data availability

All the data and relevant information are available within the Article and its Supplementary Information. Source data are provided with this paper.

Acknowledgements

D.H., C.L. and M.D.B. acknowledge support from a Defense Advanced Research Projects Agency Young Faculty Award (DARPA YFA) (D18AP00041, M.D.B.) and the National Science Foundation under the DMREF programme (award number 2119105, M.D.B.). J.F., B.L. and E.J.M. acknowledge support from Nebraska Tobacco Settlement Biomedical Research Development funds (E.J.M.). X.Y. and R.L. acknowledge support from the National Science Foundation under the DMREF programme (award number 2118878, R.L.).

Author contributions

D.H. and M.D.B. conceived the idea. D.H., C.L. and J.M.P.-G. prepared adhesives and performed experiments. J.F., B.L. and E.J.M. prepared and performed robotic arm and pulse oximetry experiments. D.H., C.L., X.Y., R.L. and M.D.B. analysed the results. D.H. and M.D.B. wrote the paper with input from E.J.M. and R.L., and M.D.B supervised the study.

Competing interests

M.D.B. and D.H. are inventors on a patent application (US patent 17/248,351) on the adhesive design. The remaining authors declare no competing interests.

Additional information

Supplementary information The online version contains supplementary material available at https://doi.org/10.1038/s41563-023-01577-2.

Correspondence and requests for materials should be addressed to Michael D. Bartlett.

Peer review information *Nature Materials* thanks Anand Jagota, Hoon Eui Jeong and the other, anonymous, reviewer(s) for their contribution to the peer review of this work.

nature portfolio

Corresponding author(s): Michael D. Bartlett

Last updated by author(s): Mar 12, 2023

Reporting Summary

Nature Portfolio wishes to improve the reproducibility of the work that we publish. This form provides structure for consistency and transparency in reporting. For further information on Nature Portfolio policies, see our Editorial Policies and the Editorial Policy Checklist.

Statistics

For all statistical analyses, confirm that the following items are present in the figure legend, table legend, main text, or Methods section.

n/a	Confirmed
☐	☒ The exact sample size (*n*) for each experimental group/condition, given as a discrete number and unit of measurement
☐	☒ A statement on whether measurements were taken from distinct samples or whether the same sample was measured repeatedly
☒	☐ The statistical test(s) used AND whether they are one- or two-sided *Only common tests should be described solely by name; describe more complex techniques in the Methods section.*
☒	☐ A description of all covariates tested
☒	☐ A description of any assumptions or corrections, such as tests of normality and adjustment for multiple comparisons
☐	☒ A full description of the statistical parameters including central tendency (e.g. means) or other basic estimates (e.g. regression coefficient) AND variation (e.g. standard deviation) or associated estimates of uncertainty (e.g. confidence intervals)
☒	☐ For null hypothesis testing, the test statistic (e.g. *F*, *t*, *r*) with confidence intervals, effect sizes, degrees of freedom and *P* value noted *Give P values as exact values whenever suitable.*
☒	☐ For Bayesian analysis, information on the choice of priors and Markov chain Monte Carlo settings
☒	☐ For hierarchical and complex designs, identification of the appropriate level for tests and full reporting of outcomes
☒	☐ Estimates of effect sizes (e.g. Cohen's *d*, Pearson's *r*), indicating how they were calculated

Our web collection on statistics for biologists contains articles on many of the points above.

Software and code

Policy information about availability of computer code

Data collection	Adhesion data was collected using commercial Instron Bluehill 3 software. Pulse oximetry data was collected using commercial MATLAB software (2020a). Finite Element Analysis (FEA) for the peeling mechanics of metamaterial adhesives was conducted using ABAQUS software (version 2020).
Data analysis	Commercial MATLAB software (2020a) was used for adhesion data analysis. Open source Tracker software (Open Source Physics, V5.1.5) was used for crack velocity analysis.

For manuscripts utilizing custom algorithms or software that are central to the research but not yet described in published literature, software must be made available to editors and reviewers. We strongly encourage code deposition in a community repository (e.g. GitHub). See the Nature Portfolio guidelines for submitting code & software for further information.

Data

Policy information about availability of data

All manuscripts must include a data availability statement. This statement should provide the following information, where applicable:

- Accession codes, unique identifiers, or web links for publicly available datasets
- A description of any restrictions on data availability
- For clinical datasets or third party data, please ensure that the statement adheres to our policy

All the data and relevant information are available within the article and Supplementary Information. Source data are provided with this paper.

Field-specific reporting

Please select the one below that is the best fit for your research. If you are not sure, read the appropriate sections before making your selection.

☒ Life sciences ☐ Behavioural & social sciences ☐ Ecological, evolutionary & environmental sciences

For a reference copy of the document with all sections, see nature.com/documents/nr-reporting-summary-flat.pdf

Life sciences study design

All studies must disclose on these points even when the disclosure is negative.

Sample size	No sample size considerations were performed.
Data exclusions	Data were non excluded from the analysis.
Replication	Adhesive characteristics were measured from 1-3 independent samples for each condition.
Randomization	This is not relevant to our study as all adhesive samples and substrates were tested in a clean and pristine state.
Blinding	Blinding was not relevant to our study as automatic analysis through MATLAB and Tracker enabled unbiased quantification of adhesive characteristics.

Reporting for specific materials, systems and methods

We require information from authors about some types of materials, experimental systems and methods used in many studies. Here, indicate whether each material, system or method listed is relevant to your study. If you are not sure if a list item applies to your research, read the appropriate section before selecting a response.

Materials & experimental systems

n/a	Involved in the study
☒	☐ Antibodies
☒	☐ Eukaryotic cell lines
☒	☐ Palaeontology and archaeology
☒	☐ Animals and other organisms
☒	☐ Human research participants
☒	☐ Clinical data
☒	☐ Dual use research of concern

Methods

n/a	Involved in the study
☒	☐ ChIP-seq
☒	☐ Flow cytometry
☒	☐ MRI-based neuroimaging